Formation of the N≡N Triple Bond from Reductive Coupling of a Paramagnetic Diruthenium Nitrido Compound

Sungho V. Park, Amanda R. Corcos, Alexander N. Jambor, Tzuhsiung Yang, and John F. Berry*

Department of Chemistry, University of Wisconsin–Madison, 1101 University Ave., Madison, WI 53706

ABSTRACT: Construction of nitrogen–nitrogen triple bonds via homocoupling of metal nitrides is an important fundamental reaction relevant to a potential *Nitrogen Economy*. Here we report that room temperature photolysis of $Ru_2(chp)_4N_3$ (chp^- = 2-chloro-6-hydroxypyridinate) in CH_2Cl_2 produces N_2 *via* reductive coupling of $Ru_2(chp)_4N$ nitrido species. Computational analysis reveals that the nitride coupling transition state (TS) features an out-of-plane 'zigzag' geometry instead of the anticipated planar zigzag TS. However, with intentional exclusion of dispersion correction, the planar zigzag TS geometry can also be found. Both the out-of-plane and planar zigzag TS geometries feature two important types of orbital interactions: (1) Donor-acceptor interactions involving intermolecular donation of a nitride lone pair into an empty Ru–N π* orbital, and (2) Ru–N π to Ru–N π* interactions derived from coupling of nitridyl radicals. The relative importance of these two interactions is quantified both at and after the TS. Our analysis shows that both interactions are important for the formation of the N–N σ bond, while radical coupling interactions dominate the formation of N–N π bonds. Comparison is made to isoelectronic Ru_2-oxo compounds. Formation of an O–O bond via bimolecular oxo coupling is not observed experimentally, and is calculated to have a much higher TS energy. The major difference between the nitrido and oxo systems stems from an extremely large driving force, ~ –500 kJ/mol, for N–N coupling vs a more modest driving force for O–O coupling, –40 to –140 kJ/mol.

Introduction

Green ammonia synthesis[1–4] and direct ammonia fuel cells[5–8] are important enabling technologies for a zero-carbon *Nitrogen Economy*.[9–13] The basic chemical foundations for each of these catalytic technologies are reactions that cleave or form the extremely strong N–N triple bond in N_2.[14–16] Recently, intriguing chemical systems have been developed in which transition metal complexes have been used to either split N_2 into metal-nitrido complexes,[17–21] or to form N_2 via the union of two metal nitrides.[22–47] Despite these processes being the reverse of each other, differing transition state geometries were originally proposed for the N_2 cleavage and formation reactions (Scheme 1, top). Morokuma and coworkers first proposed the splitting of N_2 between two Mo centers as proceeding through a planar 'zigzag' transition state with parallel nascent Mo≡N units.[48] In contrast, Ware and Taube investigated the formation of N_2 via bimolecular coupling of two terminal, ambiphilic Os≡N units and proposed an initial N–N bond-forming transition state occurring in a 'bent' geometry by attack of a nitrogen lone pair on an empty M–N π* orbital.[49] While the Ware-Taube proposal has been used to describe N_2 formation from diamagnetic late-metal nitrido compounds, including the coupling reaction of a Mo^{VI} nitride with an Os^{VI} nitride,[32] a zigzag transition state featuring coupling of nitridyl radicals is generally proposed for open-shell nitrido compounds.[25,34] Even in cases where the transition state is not interrogated, nitridyl radical coupling is often invoked as the mechanism or driving force for N_2 formation from paramagnetic nitrido compounds,[38,44] even in the case of a Mn^{VI}-nitrido compound with little spin on the N atom.[28]

Scheme 1. Top left: Planar 'zigzag' and 'bent' transition state geometries relevant to N_2 cleavage and formation reactions. Top right: Proposed orbital models for N–N bond formation. Bottom: Structures of **1** and **2**.

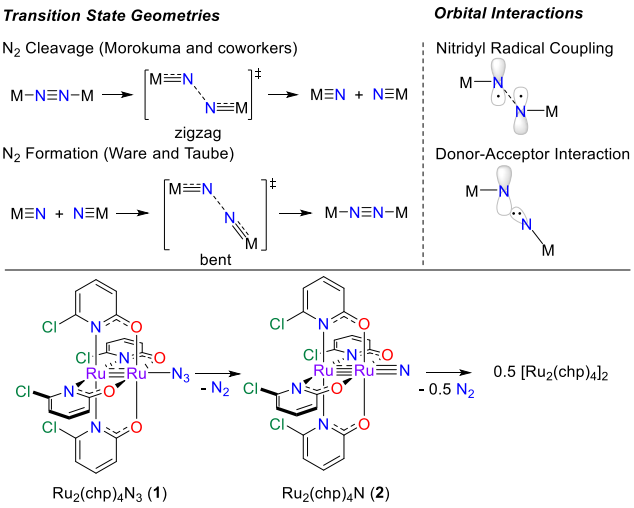

Nitride ambiphilicity, due to a high-lying N lone pair and a low-lying M–N π* orbital, is the key to the Ware-Taube mechanism, whereas a high degree of spin, population of ≥

0.5, is considered to denote nitridyl radical character and facilitate the radical coupling mechanism.[34] An assessment of the relative importance of these two orbital models is lacking and can help further efforts to design transition metal complexes with improved reactivity towards formation or cleavage of N_2.

We are interested in N_2 formation from nitrido compounds as a potential key step in catalytic ammonia oxidation.[13] Our research group has been exploring the application of metal–metal bonded Ru_2 complexes toward the *Nitrogen Economy*, and reported that the photolysis of $Ru_2(chp)_4N_3$ (**1**) (chp^- = 2-chloro-6-hydroxypyridinate; Scheme 1, bottom) produces the corresponding open-shell (S = 1/2) nitrido compound, $Ru_2(chp)_4N$ (**2**).[50] We now report that N_2 is released upon photolysis of **1** not only due to formation of **2** but also from N–N reductive coupling from dimerization of **2**. We now believe this reductive coupling reaction to be responsible for limiting our ability to perform intermolecular N atom transfer reactions from **2**.[50] In contrast to the facile formation of N_2 from **2**, the corresponding oxo intermediate, $Ru_2(chp)_4O$, was found not to release O_2.[51] The O–O bond formation reaction is, nevertheless, foundational to the mechanism of oxygen evolution, which is also an important fundamental reaction for green electrochemical synthesis of ammonia in the *Nitrogen Economy*.[52,53,54] In this work, we examine in detail the electronic structure of **2**, its reaction to produce N_2, a computational investigation into the mechanism of N_2 formation from **2**, and a thermodynamic comparison to the corresponding O–O bond formation reactions.

Results and Discussion

Electronic Structure of 2. The nitrido compound $Ru_2(chp)_4N$, **2**, was proposed in our previous work as an unstable intermediate formed upon photolysis of the azido precursor $Ru_2(chp)_4N_3$, **1**.[50] The identity of **2** was established on the basis of mass spectrometry and EPR spectroscopy experiments as an S = 1/2 nitrido species, quite distinct from the S = 3/2 azido precursor. These features also agree well with those of the $Ru_2(DPhF)_4N$ nitrido complex (DPhF = *N*,*N*′-diphenylformamidinate), which was characterized not only by mass spectrometry and EPR spectroscopy, but also by visible absorption spectroscopy, resonance Raman spectroscopy, and X-ray absorption spectroscopy including extended X-ray absorption fine structure (EXAFS) analysis.[55] Subsequently, crystallographic data for this nitrido complex were obtained.[56]

The electronic structure of **2** was not investigated in previous work, and is therefore investigated here, both at the level of density functional theory (DFT) and *ab initio* complete active space self-consistent field *N*-electron valence perturbation theory (CASSCF/NEVPT2). As **2** has not been crystallographically characterized, an initial guess for the structure was obtained by deleting the two distal N atoms from the azide group in **1**. The resulting structure was then subjected to geometry optimization under BP86/def2-TZVP, which resulted in two distinct but reasonable geometries for **2**. The two geometries feature either a bent (168°) or linear Ru–Ru–N angle. While the bent structure was found to be favored by DFT, the linear structure was lower in energy upon examination by CASSCF. We only describe the linear geometry and the CASSCF orbital picture for simplicity. The optimized Ru–Ru and Ru≡N distances are 2.43 and 1.69 Å, respectively, similar to those determined for $Ru_2(DPhF)_4N$ by EXAFS (2.42 and 1.76 Å, respectively)[55] or by crystallography (2.41 and 1.72 Å, respectively).[56]

The active space for **2** contains 15 electrons in 11 orbitals, which include the valence d_{z^2}, d_{xz}, d_{yz}, and d_{xy} orbitals of both Ru atoms and the three valence 2p orbitals of the nitrido N atom. Considering the approximate C_4 symmetry of **2**, these orbitals split into those of σ, π, and δ symmetry. Among the σ and π symmetry groups, delocalization between the two Ru atoms and the N atom leads to the formation of three-center orbitals having sets with bonding, non-bonding, and antibonding character as expected from basic molecular orbital theory. The δ symmetry orbitals only have Ru character, and the CASSCF results indicate little δ delocalization. Figure 1 shows the rough energetic ordering of these orbitals and their occupation numbers, as they are occupied by the 15 valence electrons of the $[Ru_2N]^{4+}$ system (Ru_2^{7+} with 9 valence electrons in 4d orbitals plus N^{3-} with 6 valence electrons in 2p orbitals; the N 2s orbital is not included in the active space).

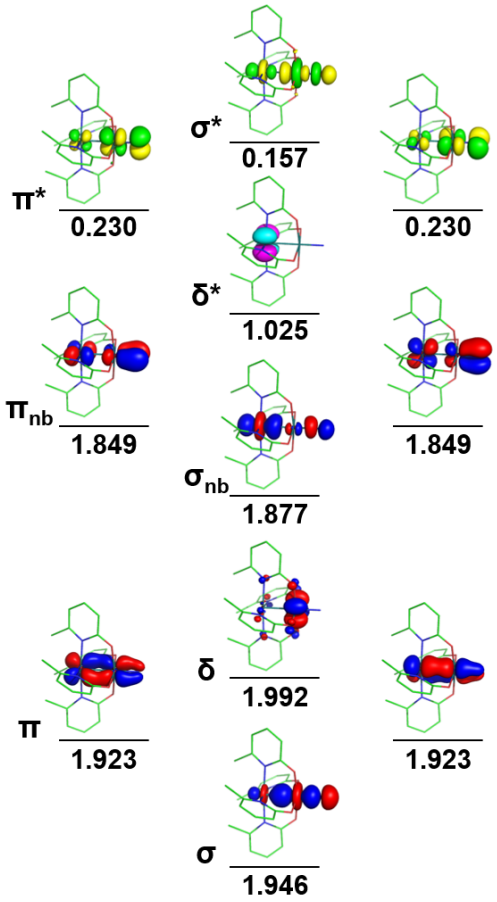

Figure 1. CASSCF(15,11) active space orbitals of doublet $Ru_2(chp)_4N$ shown with orbital occupancies. Blue/red indicates doubly occupied, magenta/cyan indicates singly occupied, and yellow/green indicates unoccupied molecular orbitals.

The occupation numbers in Figure 1 are close to the expected integer values for the $\sigma^2\pi^4\delta^2\sigma_{nb}^2\pi_{nb}^4\delta^{*1}$ configuration, and this configuration accounts for 71% of the CASSCF wavefunction. This same configuration was found to contribute to 66% of the CASSCF wavefunction in the $Ru_2(DPhF)_4N$ nitrido complex.[57] Both Ru_2-nitrido compounds may be described as having a three-center/four-electron ($3c/4e$) σ bond and two $3c/4e$ π bonds that span the Ru–Ru–N unit. The important conclusion from this electronic structure analysis is that, although **2** is an open shell nitride, its electronic structure is unlike those of paramagnetic monometallic nitrides, specifically in that the singly occupied molecular orbital (SOMO) resides on the Ru atom *trans* to the nitride. Thus, the CASSCF wavefunction indicates $|P|$ of only 0.13, where P is the spin population, for the nitrido N atom of **2**, with little nitridyl radical character.

Experimental Assessment of N–N Coupling Reactivity. Isotopic labeling was used to probe N–N coupling via the nitrido complex **2**. The labeled mixture of Ru_2-azide isomers $Ru_2(chp)_4{}^{15}NN_2$ / $Ru_2(chp)_4N_2{}^{15}N$ (**1***) was prepared by salt metathesis of $Ru_2(chp)_4Cl$[50,58] with $Na^{15}NN_2$ in a mixture of dry dichloromethane and dry methanol for five days at room temperature, from which **1*** was isolated in 85% yield after workup (Scheme 2). FT-IR spectroscopy confirms the formation of **1*** due to the presence two distinct azide stretches at 2019 cm^{-1} and 2008 cm^{-1}, isotopically shifted from 2018 cm^{-1} in unlabeled **1** (Figure S1).

Scheme 2. Formation of labelled Ru_2-azide 1* from $Ru_2(chp)_4Cl$.

$$Ru_2(chp)_4Cl + Na^{15}NN_2 \xrightarrow[\text{DCM/MeOH at RT}]{} Ru_2(chp)_4{}^{15}NN_2 \,/\, Ru_2(chp)_4N_2{}^{15}N + NaCl$$

Since **1*** is a statistical mixture of $Ru_2(chp)_4{}^{15}NN_2$ and $Ru_2(chp)_4N_2{}^{15}N$, photolysis of **1*** generates both the Ru_2-nitride intermediates $Ru_2(chp)_4N$, **2**, and its isotopomer $Ru_2(chp)_4{}^{15}N$, **2*** [50] as a statistical mixture, with ^{15}NN and N_2 as byproducts, respectively. If Ru_2-nitride intermediates **2** and **2*** were to undergo bimolecular coupling to produce dinitrogen, there would be three possible resulting isotopes (N_2, ^{15}NN, and $^{15}N_2$) distinguishable by mass spectrometry by their m/z ratios of 28, 29, and 30 amu, respectively. Scheme 3 catalogs the possible photolysis and N–N coupling outcomes, indicating that products with m/z = 28 and 29 can both be produced via either the photolysis of **1*** or nitride coupling of **2**/**2***. One mass, m/z = 30, can only arise from nitride coupling of **2*** with another **2*** molecule under this scheme, and the presence of this mass signal would therefore positively confirm nitride dimerization.

Scheme 3. Possible azide photolysis and dimerization products and their corresponding masses. Only m/z = 30 amu (shown in red) is found only from nitride dimerization and not from photolysis.

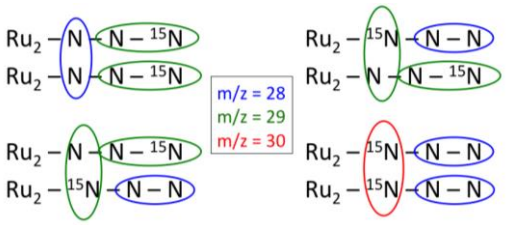

In order to determine if dinitrogen is released due to Ru_2-nitride coupling upon photolysis of **1***, we dissolved **1*** in dry dichloromethane under an atmosphere of argon and subjected it to photolytic conditions at room temperature for four hours, after which we analyzed the headspace using gas chromatography-mass spectrometry (GC-MS) analysis. Due to initial terminal loss of dinitrogen from the Ru_2-azide **1***, we anticipated measuring m/z = 28 and m/z = 29 by GC-MS for both N_2 and ^{15}NN (Scheme 3), which we confirm. We found that $^{15}N_2$ is also generated, for m/z = 30 is present in significant quantities for this reaction compared to the control of argon gas (Figure 2). This result suggests that Ru_2-nitride dimerization is possible.[50] However, this conclusion implies the assumption that photolysis proceeds completely to nitrido products and does not form azide radicals.

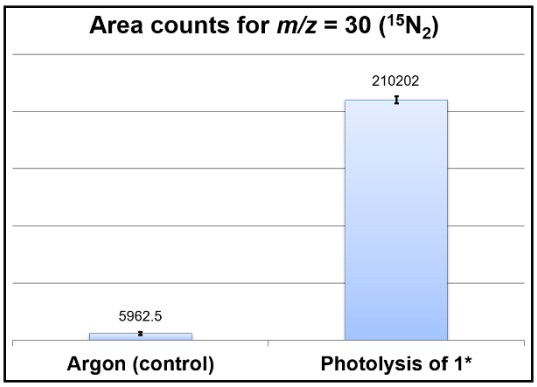

Figure 2. Headspace analysis by GC-MS after photolysis of **1*** in CH_2Cl_2 at room temperature under Ar, compared to a control of just Ar.

To rule out the possibility of photolytic azide radical formation and dimerization, which can also give the observed m/z = 30 signature, we turned to manometry measurements. There was no detectable difference between the final pressure after 4 hours of photolysis of **1** in CH_2Cl_2 under a dinitrogen atmosphere either with or without the presence of 100 equivalents of acrylamide, a known azide radical scavenger (Figure S7).[59–62] We therefore propose that room temperature photolysis does not generate azide radical, and that any nitrogen formed in this process is made via the formation of **2** and its bimolecular coupling.

Additional experiments were performed to analyze the resulting Ru product after nitride coupling of photogenerated **2**. After the 4 hour photolysis, $Ru_2(chp)_4Cl$ is detected in 5% conversion in the paramagnetic region of the NMR spectrum of the CH_2Cl_2-soluble residue (Figure S3). The dark brown material that does not dissolve in CH_2Cl_2 is assigned to dimeric $[Ru_2(chp)_4]_2$ (14% isolated yield) based on its IR signature and its NMR spectrum in d_6-DMSO, which

shows peaks that match those of $Ru_2(chp)_4(DMSO)$ (Figure S4).[13] The mass balance is improved when HCl gas is bubbled through the reaction mixture after the photolysis, with $Ru_2(chp)_4Cl$ recovered in 40% conversion. In this case, however, the CH_2Cl_2-insoluble brown powder does not give NMR signals attributable to any Ru_2 species upon dissolving in d_6-DMSO and is also MALDI and ESI-MS silent, hence it is attributed to polymeric $(RuCl_3)_x$. Based on these results, we propose the following reaction pathway for the generation of N_2 via nitride coupling of photogenerated **2**. In the absence of HCl(g), the resulting reduced $Ru_2(chp)_4$ species appears to abstract a chlorine atom from CH_2Cl_2 in a process similar to that proposed for Rh_2 species.[63]

Scheme 4. Proposed mechanism for the formation of N_2 from photolysis of 1.

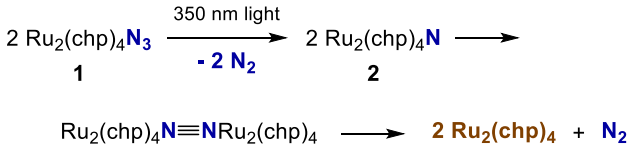

Further support for this pathway was found when the photolysis was conducted in the presence of excess DMPO (5,5-dimethyl-1-pyrroline *N*-oxide), which is another radical trapping agent that we tested. The proposed $Ru_2(chp)_4$ species at the end of Scheme 4 can be trapped in the form of $Ru_2(chp)_4(DMPO)$, which has been crystallographically characterized (Figure 3).

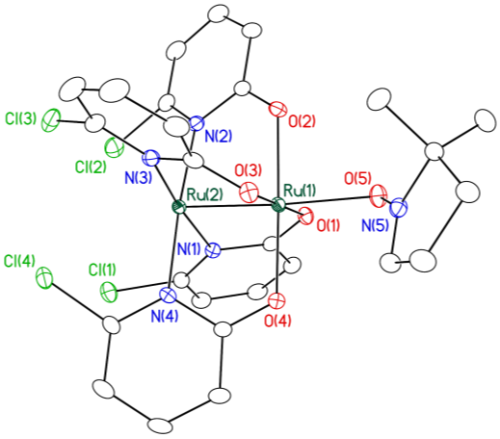

Figure 3. Crystal structure of $Ru_2(chp)_4(DMPO)$ shown with thermal ellipsoids drawn at the 50% probability level. Hydrogen atoms and solvent molecule are omitted for clarity.

Computational Analysis of N–N Bond Formation. To gain further insights into the nitride coupling reaction pathway, we turned to computational methods, specifically ωB97X-D3/def2-SVP(TZVPP on Ru). Upon allowing two molecules of **2** to approach each other in two trajectories along the singlet, triplet, quintet and septet spin surfaces, we found that the lowest energy TS is on the triplet spin surface, featuring an out-of-plane zigzag geometry with a long N···N distance of 2.88 Å and a Ru–N–N–Ru dihedral angle of 80.° (Figure 4). The two Ru–N···N angles are similar, at 112° and 117°, suggesting symmetric orbital interactions between the two nitrido compounds. Our finding of an out-of-plane zigzag TS geometry is particularly surprising considering that only planar zigzag TS geometries have been considered since Morokuma's original proposal for N–N cleavage,[17,19,21,34,36,39,64–78] with the exception of Schneider's report of two out-of-plane zigzag TS geometries with M–N–N–M dihedral angles of 142° and 152° for the coupling of iridium nitrido complexes.[25]

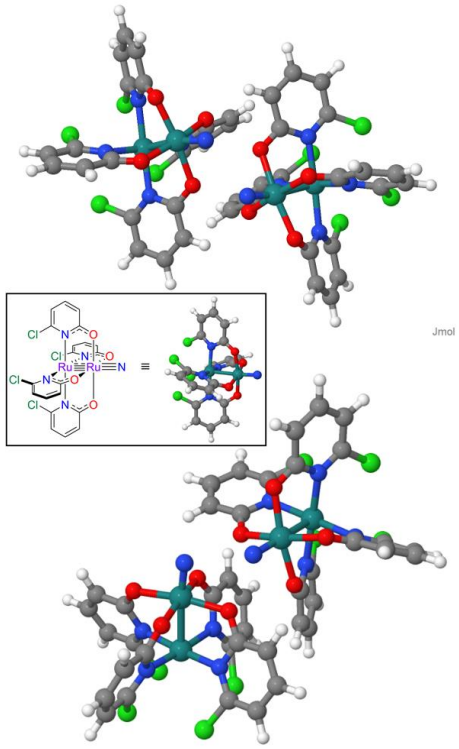

Figure 4. Two views of the triplet out-of-plane zigzag TS geometry in the homocoupling reaction of **2**.

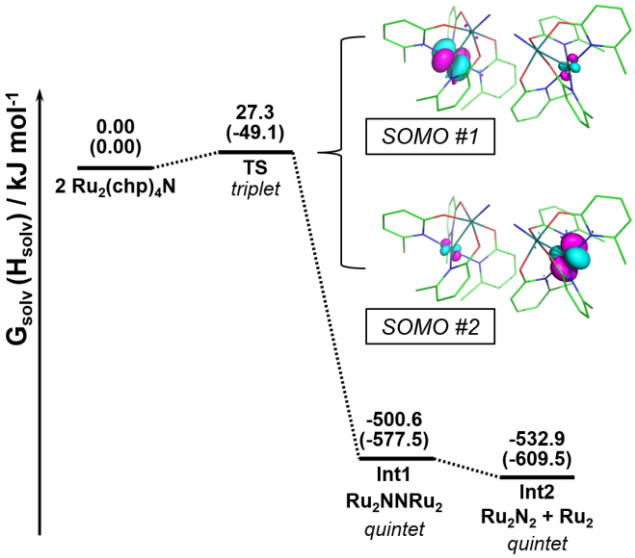

Figure 5. Computed reaction coordinate diagram for the homocoupling reaction of **2**. Inset shows the two SOMOs of the triplet out-of-plane zigzag TS.

The N–N reductive coupling reaction features an early transition state (TS) that resembles the parent nitrido complex in terms of energy and spin population. The reaction proceeds through a triplet TS, ultimately undergoing a spin transition to yield a quintet bridging dinitrogen complex (Int1, Figure 5). Based on the spin populations (Figure S9), this bridging dinitrogen complex appears to be best described as consisting of two $S = 1$ Ru_2^{4+} units with a bridging neutral dinitrogen ligand. Further cleavage of a Ru–N bond from the bridging N_2 complex forming Int2 *en route* to elimination of N_2 is barrierless.

The out-of-plane zigzag transition state geometry is different from either the planar zigzag or the planar bent geometries that have previously been proposed by Morokuma and Taube, respectively (Scheme 1). We attribute the stability of the out-of-plane zigzag geometry to weak, non-bonding van der Waals interactions involving the ligand environment. Importantly, such interactions were not considered by Morokuma and coworkers, as such effects were not included in DFT calculations at the time.[48] In fact, for the N–N coupling of **2**, we were able to optimize to the planar, Morokuma-type zigzag transition state when dispersion correction (D3) was intentionally omitted from the calculations. Based on the single point energies, we observe that the out-of-plane zigzag TS is favored by ~ 60 kJ/mol due to favorable π-π interactions between the pyridine rings in the ligand backbone (Table 1). The importance of the dispersion correction in these calculations is further demonstrated by the observation that when the planar zigzag structures are reoptimized *with* D3, the structure immediately collapses to an out-of-plane structure to enable noncovalent interactions between the equatorial ligands of the two nitrido compounds.

Table 1. Single point energies (SPE) of the out-of-plane and planar zigzag transition states along the triplet and broken symmetry (BS) singlet spin surfaces. Values are in kJ/mol.

	Rel. SPE with dispersion correction	Rel. SPE without dispersion correction
Triplet out-of-plane zigzag	0.0 (reference)	0.0 (reference)
Triplet planar zigzag	57.4	-3.7
BS singlet out-of-plane zigzag	21.8	20.2
BS singlet planar zigzag	58.3	-3.7

To probe the electronic driving force for N–N bond formation, the orbital interactions present in the two TS geometries were examined using natural bond orbital (NBO) methods for the broken symmetry (BS) singlet and triplet states. NBO analysis reveals two types of donor-acceptor interactions present in these transition states: N lone pair to Ru–N π* and Ru–N π to Ru–N π* (Figure 6). The former interaction is reminiscent of the orbital model for N–N bond formation proposed by Burger and earlier by Taube,[36,49] in which the nitrogen lone pair derives from either a nitrogen *s* or a *p* orbital. The Ru–N π to Ru–N π* interaction, shown at the bottom of Figure 6, may be interpreted as a component that can be linearly combined with another equivalent interaction in the opposite direction to give the nitridyl radical coupling model. Thus, the NBO analysis in this case allows us to quantify the degree to which either nitride ambiphilicity or nitridyl radical coupling contributes to the overall N–N bond forming step.

The donor-acceptor interactions present in the out-of-plane and planar zigzag TS structures in either the triplet or the BS singlet state are all qualitatively similar and the interactions with the largest stabilization energy are found in the singlet out-of-plane zigzag geometry, where the N···N distance is the shortest at 2.34 Å (see Table S3 for comparisons). Since nitride coupling is a highly exothermic reaction (ΔG = -501 kJ/mol) with an early TS, the magnitude of the donor-acceptor interactions between the two nitride molecules that contribute to the TS energy are rather small. Furthermore, the energy difference between the donor N(s) lone pair and the acceptor Ru–N π* orbital is calculated to be very large, at 17.4 eV. Nevertheless, it is remarkable that the N lone pair → Ru–N π* interaction is the dominant interaction in all cases including the planar zigzag TS geometries, despite a nitride spin population, *P*, that can range from $|P| = 0.14$ to $|P| = 0.63$ based the method of DFT used (see Table S4; $|P| = 0.13$ based on CASSCF). This implies that DFT may overestimate nitridyl radical character and that these values must be interpreted with caution.

To elucidate the donor-acceptor interactions present at other points along the reaction coordinate, NBO calculations were conducted for each point along the entire intrinsic reaction coordinate (IRC) for the lowest energy path, which proceeds through the triplet out-of-plane zigzag TS (a total of 37 points). Neither of the two N–N interaction types discussed above were detected prior to the TS or after the point in the IRC when the N–N distance had closed to 1.30 Å (N–N Mayer bond order of 1.91) (Figure 7). As the reaction progresses *after* the TS, radical coupling interactions continually become stronger, whereas the magnitude of the N lone pair → Ru–N π* interaction reaches a maximum at a N–N distance of 1.54 Å and then decreases afterwards (Figure 7). Between N–N Mayer bond orders of 0 and 1, the two interactions have similar energetic contributions; however, while the N–N bond order increases from 1 to 2, the N lone pair → Ru–N π* interaction becomes less important than the Ru–N π → Ru–N π* interaction. This suggests that, while both nitride ambiphilicity and nitridyl radical character are important in defining the TS, the radical coupling type interaction increases in importance for the thermodynamic driving force of the reaction *after* the TS. Since progression from the TS to a N–N Mayer bond order of 1.91 also accompanies an increase in the Ru–N bond distance from 1.67 Å to 1.92 Å, the observed increase in radical coupling interactions agrees with Bendix and coworkers' description of increased nitridyl radical character upon elongation of the Cr≡N bond.[79] However, at a N–N Mayer bond order of 1.91, the calculated nitride spin populations

are actually diminished, with values of $|P|$ = 0.27 and 0.20 (vs $|P|$ = 0.52 and 0.59 at the TS). This implies that nitride spin population alone cannot be used to pinpoint which of the two interactions are dominant, and reiterates our previous argument on the need to interpret DFT-calculated spin populations with caution.

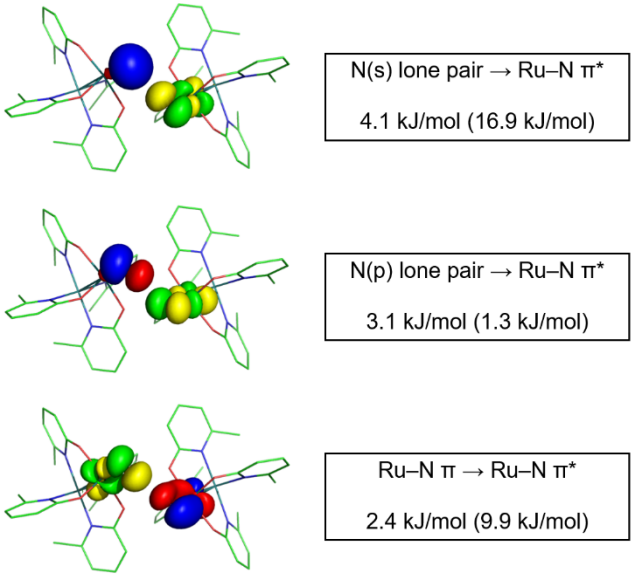

Figure 6. NBO depictions of selected donor-acceptor interactions present in the triplet out-of-plane zigzag TS. Donor orbitals are depicted in blue/red and acceptor orbitals in green/yellow. The type of interaction and sum of its stabilization energies over all equivalent interactions are listed in the adjacent boxes (values in parentheses indicate the analogous sum for the triplet planar zigzag TS).

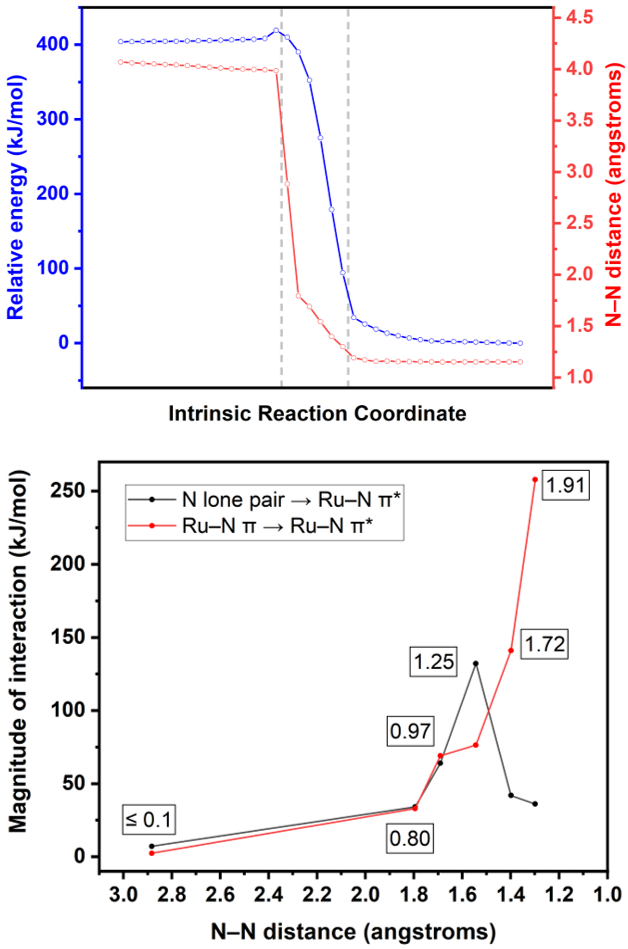

Figure 7. Out of 37 points along the IRC, only the six that are within the two gray dashed lines (top graph) display N lone pair → Ru–N π and Ru–N π → Ru–N π* interactions. The magnitude of these interactions, along with N–N Mayer bond orders in boxes, are shown in the bottom graph.

At the TS, NBO analysis suggests that both types of interactions facilitate the formation of the N–N σ bond, as seen in the depictions in Figure 6. Even the orbitals of Ru–N π symmetry are aligned such that σ overlap is possible between the donor and acceptor orbitals. However, as the reaction progresses, the N(p) lone pair → Ru–N π* and Ru–N π → Ru–N π* interactions change directionality such that N–N π type overlap becomes accessible at shorter N–N distances, leading to the formation of the N–N π bond (Figure 8). The increased contribution from the radical coupling interaction later in the reaction coordinate can be rationalized in terms of the relative energies of the donor orbitals (Figure 8, left) since the N(p) lone pair orbitals are closer to the Ru–N π* orbital in energy at the TS, leading its initial larger contribution. But as the N–N bond distance contracts further, the Ru–N π orbitals are now able to contribute more to the formation of the N–N π bond. The N(s) lone pair does not have the correct orbital symmetry for π bond formation, and only contributes to the formation of the N–N σ bond.

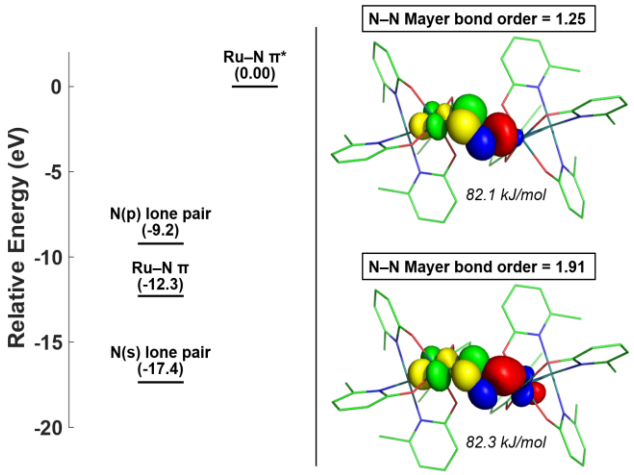

Figure 8. (Left) Energy diagram depicting the relative energies of the donor and acceptor orbitals computed at the out-of-plane triplet zigzag TS. (Right) N(p) lone pair → Ru–N π* and Ru–N π → Ru–N π* interactions involved in the formation of the N–N π bond.

Our NBO analysis encouraged us to revisit Ware and Taube's original depiction of the orbital interaction present in the planar bent geometry, which is only one out of many possible orbital interactions that may be operational. At least for homocoupling of a single nitride species, the donor-acceptor interaction must be present in *both* directions, which is what we observe for NBO calculations of both the planar zigzag and out-of-plane zigzag TS geometries in the homocoupling of **2**. We do not see evidence of significantly asymmetric donor-acceptor interactions either in the NBO analysis or in the optimized transition state structures. We have attempted to locate the planar bent transition states using constrained optimizations but were not successful due to the collapsing of the structures. The reason for our TS deviating from planar bent to out-of-plane zigzag could also be attributable to π-π stacking interactions of the pyridine rings, but the symmetric nature of the donor-acceptor interactions involved in N–N bond formation (e.g., N(lp) → M–N(π*) = M–N(π*) ← N(lp)) point to the necessity of a more symmetric TS structure than that proposed by Ware and Taube.

In 2012, we outlined the reactivity consequences of bimetallic vs monometallic nitrido complexes,[57] some of which are manifest in the current work. Specifically, lower transition state energies are expected for metal-metal-nitrido reactivity, as well as a higher density of states as compared to monometallic nitrido species. Regarding the transition state energy, it is useful to compare the system described here to the monometallic Rh-nitrido system supported by the "PNP" ligand N(CHCHPtBu$_2$)$_2$ reported by de Bruin and Schneider.[38] The mono-Rh nitrido compound has an N–N coupling TS energy calculated to be about twice that of the Ru–Ru nitrido complex **2**. Furthermore, while only one spin state was investigated for Rh (with the others presumably prohibitively high in energy), the Ru$_2$ system has four different spin states that all lie within ~ 70 kJ/mol of each other; we would not, *a priori*, have expected the triplet surface to be favored. The metal-metal bonded nitrido system in this case acts more like a monometallic first-row transition metal complex than the mononuclear Rh example. For example, N–N coupling via paramagnetic Fe(V) nitrido complexes is calculated to be barrierless.[44]

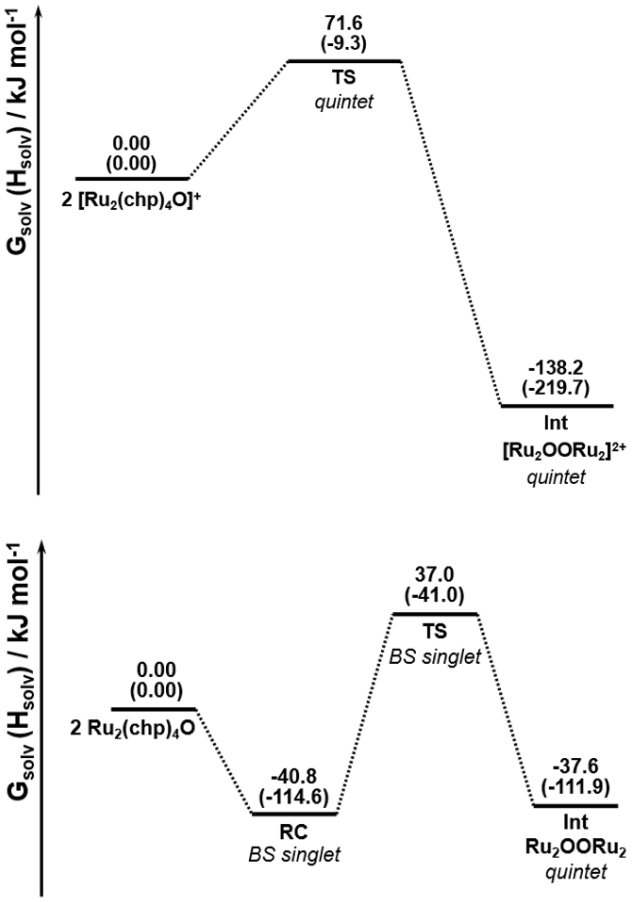

Figure 9. Computed reaction coordinate diagrams for the homocoupling of [Ru$_2$(chp)$_4$O]$^+$ (top) and for the homocoupling of Ru$_2$(chp)$_4$O (bottom). The numbers on top show the G values computed with the CPCM(CH$_2$Cl$_2$) solvation model (G_{solv}) with the analogous H_{solv} values shown below in parentheses (units are in kJ/mol).

Computational Comparison to O–O Bond Formation. We also examined the analogous homocoupling reaction of oxo species [Ru$_2$(chp)$_4$O]$^+$ (**3**) and Ru$_2$(chp)$_4$O (**4**), the former being isoelectronic to **2**. These reactions both show higher barriers of activation as compared to the nitride system (Figure 9). In the case of **3**, the high TS energy is mainly attributable to coulombic repulsion effects. Experimentally, photolysis of Ru$_2$(chp)$_4{}^{18}$O^{18}O$_2$ has been reported to form the transient Ru$_2$-oxo species **4** without production of ^{18}O$_2$,[51] which is consistent with the effective barrier of ~ 78 kJ/mol calculated for O–O coupling from **4**. A major difference between the O–O coupling and N–N coupling reactions is the significantly smaller thermodynamic driving force for the former reaction (–37.6 kJ/mol for O–O coupling in **4** vs –500.6 kJ/mol for N–N coupling in **2**). Interestingly, Ru$_2$(chp)$_4$ species in the Ru$_2^{4+}$ oxidation state are known to be oxidized by O$_2$.[80,81] The results presented here indicate

that this reactivity likely does not involve bimolecular O–O cleavage, consistent with the observation of reversible O_2 binding to Ru_2 complexes supported by amidinate ligands.[82]

Summary

In this work, we have shown that photogenerated **2** produces N_2 via bimolecular reductive coupling, and we have examined the associated nitride coupling mechanism computationally. The Ware-Taube description for the nitride coupling geometry seems unlikely, at least for homobimetallic coupling, as the transition states investigated here feature symmetric out-of-plane zigzag geometries. The metal–metal bond facilitates this reaction through electron delocalization among the Ru and nitride atoms via $3c/4e$ bonds, which leads to a high degree of nitride ambiphilicity and allows multiple spin state reactivity to operate. The result is a low-energy triplet transition state for N–N σ bond formation in which both nitride ambiphilicity and nitridyl radical character contribute equally. DFT-determined nitridyl radical character in the ground state of the complex does not necessarily imply a nitridyl radical coupling mechanism, and from our IRC/NBO studies we conclude that radical coupling becomes more important after the transition state, particularly for N–N π bond formation. Analogous O–O bond formation via oxo intermediates is not favored, mainly due to the lower reaction driving force. We have identified dispersion interactions as an important factor that reduces the activation barrier for the nitride coupling reaction. We therefore believe that employing ligands that maximize dispersion interactions, while maintaining steric accessibility of the axial sites, can be a useful approach for designing molecular catalysts that can facilitate the N–N and O–O coupling reactions in a proposed *Nitrogen Economy*.

ASSOCIATED CONTENT

Supporting Information. The Supporting Information is available free of charge via the Internet at http://pubs.acs.org.
Experimental details, characterization data, and computational methods (PDF)
Accession Codes
CCDC 2127981 contains the supplementary crystallographic data for this paper. This data can be obtained free of charge via www.ccdc.cam.ac.uk/data_request/cif, or by emailing data_request@ccdc.cam.ac.uk, or by contacting The Cambridge Crystallographic Data Centre, 12 Union Road, Cambridge CB2 1EZ, UK; fax: +44 1223 336033.

AUTHOR INFORMATION

Corresponding Author

*berry@chem.wisc.edu

Author Contributions

All authors have given approval to the final version of the manuscript.

Notes

The authors declare no competing financial interest.

ACKNOWLEDGMENT

We thank the U.S. Department of Energy, Chemical Sciences, Geosciences, and Biosciences Division, Office of Basic Energy Sciences, Office of Science (DE-SC0021021). A.R.C. thanks the National Science Foundation for a Graduate Research Fellowship (DGE-0718123). We thank Amelia Wheaton for assistance with X-ray crystallography. We gratefully acknowledge the Center for High Throughput Computing (CHTC) at the UW-Madison for providing computational resources and assistance. The NMR facilities and the X-ray crystallography facilities were supported by a generous gift from Paul J. and Margaret M. Bender; the NMR facilities were additionally supported by the NIH (S10 OD012245).

REFERENCES

1. Bhattacharya, P.; Prokopchuk, D. E.; Mock, M. T. Exploring the Role of Pendant Amines in Transition Metal Complexes for the Reduction of N_2 to Hydrazine and Ammonia. *Coord. Chem. Rev.* **2017**, *334*, 67–83.
2. Chen, J. G.; Crooks, R. M.; Seefeldt, L. C.; Bren, K. L.; Bullock, R. M.; Darensbourg, M. Y.; Holland, P. L.; Hoffman, B.; Janik, M. J.; Jones, A. K.; Kanatzidis, M. G.; King, P.; Lancaster, K. M.; Lymar, S. V.; Pfromm, P.; Schneider, W. F.; Schrock, R. R. Beyond Fossil Fuel-Driven Nitrogen Transformations. *Science* **2018**, *360*, eaar6611.
3. Floeser, B. M.; Tuczek, F. Synthetic Nitrogen Fixation with Mononuclear Molybdenum Complexes: Electronic-Structural and Mechanistic Insights from DFT. *Coord. Chem. Rev.* **2017**, *345*, 263–280.
4. Tang, C.; Qiao, S. Z. How to Explore Ambient Electrocatalytic Nitrogen Reduction Reliably and Insightfully. *Chem. Soc. Rev.* **2019**, *48*, 3166–3180.
5. Fukuzumi, S. Production of Liquid Solar Fuels and Their Use in Fuel Cells. *Joule* **2017**, *1*, 689–738.
6. Siddharth, K.; Chan, Y.; Wang, L.; Shao, M. Ammonia Electrooxidation Reaction: Recent Development in Mechanistic Understanding and Electrocatalyst Design. *Curr. Opin. Electrochem.* **2018**, *9*, 151–157.
7. Zhao, Y.; Setzler, B. P.; Wang, J.; Nash, J.; Wang, T.; Xu, B.; Yan, Y. An Efficient Direct Ammonia Fuel Cell for Affordable Carbon-Neutral Transportation. *Joule* **2019**, *3*, 2472–2484.
8. Dunn, P. L.; Cook, B. J.; Johnson, S. I.; Appel, A. M.; Bullock, R. M. Oxidation of Ammonia with Molecular Complexes. *J. Am. Chem. Soc.* **2020**, *142*, 17845–17858.
9. Adli, N. M.; Zhang, H.; Mukherjee, S.; Wu, G. Ammonia Oxidation Electrocatalysis for Hydrogen Generation and Fuel Cells. *J. Electrochem. Soc.* **2018**, *165*, J3130–J3147.
10. Lan, R.; Irvine, J. T.; Tao, S. Ammonia and Related Chemicals as Potential Indirect Hydrogen Storage Materials. *Int. J. Hydrogen Energy* **2012**, *37*, 1482–1494.
11. Elishav, O.; Lewin, D. R.; Shter, G. E.; Grader, G. S. The Nitrogen Economy: Economic Feasibility Analysis of Nitrogen-Based Fuels as Energy Carriers. *Appl. Energy* **2017**, *185*, 183–188.
12. MacFarlane, D. R.; Cherepanov, P. V.; Choi, J.; Suryanto, B. H.; Hodgetts, R. Y.; Bakker, J. M.; Ferrero Vallana, F. M.; Simonov, A. N. A Roadmap to the Ammonia Economy. *Joule* **2020**, *4*, 1186–1205.
13. Trenerry, M. J.; Wallen, C. M.; Brown, T. R.; Park, S. V.; Berry, J. F. Spontaneous N_2 Formation by a Diruthenium Complex Enables Electrocatalytic and Aerobic Oxidation of Ammonia. *Nat. Chem.* **2021**, *13*, 1221–1227.
14. Collman, J. P.; Hutchison, J. E.; Ennis, M. S.; Lopez, M. A.; Guilard, R. Reduced Nitrogen Hydride Complexes of a Cofacial Metallodiporphyrin and Their Oxidative Interconversion. An Analysis of Ammonia Oxidation and Prospects for a Dinitrogen Electroreduction Catalyst Based on Cofacial Metallodiporphyrins. *J. Am. Chem. Soc.* **1992**, *114*, 8074–8080.

15. Zott, M. D.; Garrido-Barros, P.; Peters, J. C. Electrocatalytic Ammonia Oxidation Mediated by a Polypyridyl Iron Catalyst. *ACS Catal.* **2019**, *9*, 10101–10108.
16. Zott, M. D.; Peters, J. C. Enhanced Ammonia Oxidation Catalysis by a Low-Spin Iron Complex Featuring Cis Coordination Sites. *J. Am. Chem. Soc.* **2021**, *143*, 7612–7616.
17. Lindley, B. M.; van Alten, R. S.; Finger, M.; Schendzielorz, F.; Würtele, C.; Miller, A. J. M.; Siewert, I.; Schneider, S. Mechanism of Chemical and Electrochemical N_2 Splitting by a Rhenium Pincer Complex. *J. Am. Chem. Soc.* **2018**, *140*, 7922–7935.
18. Laplaza, C. E.; Cummins, C. C. Dinitrogen Cleavage by a Three-Coordinate Molybdenum(III) Complex. *Science* **1995**, *268*, 861–863.
19. Laplaza, C. E.; Johnson, M. J. A.; Peters, J. C.; Odom, A. L.; Kim, E.; Cummins, C. C.; George, G. N.; Pickering, I. J. Dinitrogen Cleavage by Three-Coordinate Molybdenum(III) Complexes: Mechanistic and Structural Data. *J. Am. Chem. Soc.* **1996**, *118*, 8623–8638.
20. Forrest, S. J.; Schluschaß, B.; Yuzik-Klimova, E. Y.; Schneider, S. Nitrogen Fixation via Splitting into Nitrido Complexes. *Chem. Rev.* **2021**, *121*, 6522–6587.
21. Schluschaß, B.; Borter, J. H.; Rupp, S.; Demeshko, S.; Herwig, C.; Limberg, C.; Maciulis, N. A.; Schneider, J.; Würtele, C.; Krewald, V.; Schwarzer. D.; Schneider, S. Cyanate Formation via Photolytic Splitting of Dinitrogen. *JACS Au* **2021**, *1*, 879–894.
22. Coia, G. M.; Demadis, K. D.; Meyer, T. J. Oxidation of Ammonia in Osmium Polypyridyl Complexes. *Inorg. Chem.* **2000**, *39*, 2212–2223.
23. Man, W. L.; Chen, G.; Yiu, S. M.; Shek, L.; Wong, W. Y.; Wong, W. T.; Lau, T. C. Formation of μ-Dinitrogen (Salen)osmium Complexes via Ligand-Induced N···N Coupling of (Salen)osmium(VI) Nitrides. *Dalton Trans.* **2010**, *39*, 11163–11170.
24. Miyazaki, T.; Tanaka, H.; Tanabe, Y.; Yuki, M.; Nakajima, K.; Yoshizawa, K.; Nishibayashi, Y. Cleavage and Formation of Molecular Dinitrogen in a Single System Assisted by Molybdenum Complexes Bearing Ferrocenyldiphosphine. *Angew. Chem., Int. Ed.* **2014**, *53*, 11488–11492.
25. Abbenseth, J.; Finger, M.; Würtele, C.; Kasanmascheff, M.; Schneider, S. Coupling of Terminal Iridium Nitrido Complexes. *Inorg. Chem. Front.* **2016**, *3*, 469–477.
26. Keener, M.; Peterson, M.; Hernández Sánchez, R.; Oswald, V. F.; Wu, G.; Ménard, G. Towards Catalytic Ammonia Oxidation to Dinitrogen: A Synthetic Cycle by Using a Simple Manganese Complex. *Chem. – Eur. J.* **2017**, *23*, 11479–11484.
27. MacLeod, K. C.; Vinyard, D. J.; Holland, P. L. A Multi-iron System Capable of Rapid N_2 Formation and N_2 Cleavage. *J. Am. Chem. Soc.* **2014**, *136*, 10226–10229.
28. Clarke, R. M.; Storr, T. Tuning Electronic Structure to Control Manganese Nitride Activation. *J. Am. Chem. Soc.* **2016**, *138*, 15299–15302.
29. Man, W. L.; Tang, T. M.; Wong, T. W.; Lau, T. C.; Peng, S. M.; Wong, W. T. Highly Electrophilic (Salen)ruthenium(VI) Nitrido Complexes. *J. Am. Chem. Soc.* **2004**, *126*, 478–479.
30. Man, W. L.; Kwong, H. K.; Lam, W. W.; Xiang, J.; Wong, T. W.; Lam, W. H., Wong, W. T.; Peng, S. M.; Lau, T. C. General Synthesis of (Salen)ruthenium(III) Complexes via N···N Coupling of (Salen)ruthenium(VI) Nitrides. *Inorg. Chem.* **2008**, *47*, 5936–5944.
31. Chantarojsiri, T.; Reath, A. H.; Yang, J. Y. Cationic Charges Leading to an Inverse Free-Energy Relationship for N–N Bond Formation by Mn^{VI} Nitrides. *Angew. Chem., Int. Ed.* **2018**, *57*, 14037–14042.
32. Seymore, S. B.; Brown, S. N. Polar Effects in Nitride Coupling Reactions. *Inorg. Chem.* **2002**, *41*, 462–469.
33. Konnick, M. M.; Bischof, S. M.; Ess, D. H.; Periana, R. A.; Hashiguchi, B. G. Base Accelerated Generation of N_2 and NH_3 from an Osmium Nitride. *J. Mol. Catal. A* **2014**, *382*, 1–7.
34. Scheibel, M. G.; Askevold, B.; Heinemann, F. W.; Reijerse, E. J.; de Bruin, B.; Schneider, S. Closed-shell and Open-shell Square-planar Iridium Nitrido Complexes. *Nat. Chem.* **2012**, *4*, 552–558.
35. Lam, H. W.; Che, C. M.; Wong, K. Y. Photoredox Properties of $[OsN(NH_3)_4]^{3+}$ and Mechanism of Formation of $[\{Os(NH_3)_4(CH_3CN)\}_2N_2]^{5+}$ through a Nitrido-coupling Reaction. *J. Chem. Soc., Dalton Trans.* **1992**, 1411–1416.
36. Schöffel, J.; Šušnjar, N.; Nückel, S.; Sieh, D.; Burger, P. 4d vs. 5d – Reactivity and Fate of Terminal Nitrido Complexes of Rhodium and Iridium. *Eur. J. Inorg. Chem.* **2010**, 4911–4915.
37. Johnson, S. I.; Heins, S. P.; Klug, C. M.; Wiedner, E. S.; Bullock, R. M.; Raugei, S. Design and Reactivity of Pentapyridyl Metal Complexes for Ammonia Oxidation. *Chem. Commun.* **2019**, *55*, 5083–5086.
38. Scheibel, M. G.; Wu, Y.; Stückl, A. C.; Krause, L.; Carl, E.; Stalke, D.; de Bruin, B.; Schneider, S. Synthesis and Reactivity of a Transient, Terminal Nitrido Complex of Rhodium. *J. Am. Chem. Soc.* **2013**, *135*, 17719–17722.
39. Scheibel, M. G.; Abbenseth, J.; Kinauer, M.; Heinemann, F. W.; Würtele, C.; de Bruin, B.; Schneider, S. Homolytic N–H Activation of Ammonia: Hydrogen Transfer of Parent Iridium Ammine, Amide, Imide, and Nitride Species. *Inorg. Chem.* **2015**, *54*, 9290–9302.
40. Kane-Maguire, L. A.; Sheridan, P. S.; Basolo, F.; Pearson, R. G. Azidoruthenium(III) Complexes as Precursors for Molecular Nitrogen and Nitrene Complexes. *J. Am. Chem. Soc.* **1970**, *92*, 5865–5872.
41. Buhr, J. D.; Taube, H. Oxidation of $[Os(NH_3)_5CO]^{2+}$ to $[(Os(NH_3)_4CO)_2N_2]^{4+}$. *Inorg. Chem.* **1979**, *18*, 2208–2212.
42. Che, C. M.; Lam, H. W.; Tong, W. F.; Lai, T. F.; Lau, T. C. Model Reactions for Nitrogen Fixation. Photo-induced Formation and X-ray Crystal Structure of $[Os_2(NH_3)_8(MeCN)_2(N_2)]^{5+}$ from $[Os^{VI}(NH_3)_4N]^{3+}$. *J. Chem. Soc., Chem. Commun.* **1989**, 1883–1884.
43. Demadis, K. D.; Meyer, T. J.; White, P. S. Localization in *trans*,*trans*-$[(tpy)(Cl)_2Os^{III}(N_2)Os^{II}(Cl)_2(tpy)]^+$ (tpy = 2,2′:6′,2″-Terpyridine). *Inorg. Chem.* **1997**, *36*, 5678–5679.
44. Krahe, O.; Bill, E.; Neese, F. Decay of Iron(V) Nitride Complexes By a N–N Bond-Coupling Reaction in Solution: A Combined Spectroscopic and Theoretical Analysis. *Angew. Chem., Int. Ed.* **2014**, *53*, 8727–8731.
45. Hendrich, M. P.; Gunderson, W.; Behan, R. K.; Green, M. T.; Mehn, M. P.; Betley, T. A.; Lu, C. C.; Peters, J. C. On the Feasibility of N_2 Fixation via a Single-site Fe^I/Fe^{IV} Cycle: Spectroscopic Studies of $Fe^I(N_2)Fe^I$, $Fe^{IV}{\equiv}N$, and Related Species. *Proc. Natl. Acad. U. S. A.* **2006**, *103*, 17107–17112.
46. Betley, T. A.; Peters, J. C. A Tetrahedrally Coordinated $L_3Fe{-}N_x$ Platform that Accommodates Terminal Nitride ($Fe^{IV}{\equiv}N$) and Dinitrogen ($Fe^I{-}N_2{-}Fe^I$) Ligands. *J. Am. Chem. Soc.* **2004**, *126*, 6252–6254.
47. Ishitani, O.; White, P. S.; Meyer, T. J. Formation of Dinitrogen by Oxidation of $[(bpy)_2(NH_3)RuORu(NH_3)(bpy)_2]^{4+}$. *Inorg. Chem.* **1996**, *35*, 2167–2168.
48. Cui, Q.; Musaev, D. G.; Svensson, M.; Sieber, S.; Morokuma, K. N_2 Cleavage by Three-Coordinate Group 6 Complexes. W(III) Complexes Would Be Better Than Mo(III) Complexes. *J. Am. Chem. Soc.* **1995**, *117*, 12366–12367.
49. Ware, D. C.; Taube, H. Substitution-Induced N–N Coupling for Nitride Coordinated to Osmium(VI). *Inorg. Chem.* **1991**, *30*, 4605–4610.
50. Corcos, A. R.; Musch Long, A. K.; Guzei, I. A.; Berry, J. F. A Synthetic Cycle for Nitrogen Atom Transfer Featuring a Diruthenium Nitride Intermediate. *Eur. J. Inorg. Chem.* **2013**, 3808–3811.

51. Corcos, A. R.; Pap, J. S.; Yang, T.; Berry, J. F. A Synthetic Oxygen Atom Transfer Photocycle from a Diruthenium Oxyanion Complex. *J. Am. Chem. Soc.* **2016**, *138*, 10032–10040.
52. Giddey, S.; Badwal, S. P. S.; Kulkarni, A. Review of Electrochemical Ammonia Production Technologies and Materials. *Int. J. Hydrog. Energy* **2013**, *38*, 14576–14594.
53. Guo, X.; Zhu, Y.; Ma, T. Lowering Reaction Temperature: Electrochemical Ammonia Synthesis by Coupling Various Electrolytes and Catalysts. *J. Energy Chem.* **2017**, *26*, 1107–1116.
54. Imamura, K.; Kubota, J. Electrochemical Membrane Cell for NH_3 Synthesis from N_2 and H_2O by Electrolysis at 200 to 250 °C Using a Ru Catalyst, Hydrogen-Permeable Pd Membrane and Phosphate-Based Electrolyte. *Sustainable Energy Fuels* **2018**, *2*, 1278–1286.
55. Pap, J. S.; DeBeer George, S.; Berry, J. F. Delocalized Metal–Metal and Metal–Ligand Multiple Bonding in a Linear Ru–Ru≡N Unit: Elongation of a Traditionally Short Ru≡N Bond. *Angew. Chem., Int. Ed.* **2008**, *47*, 10102–10105.
56. Das, A.; Reibenspies, J. H.; Chen, Y. S.; Powers, D. C. Direct Characterization of a Reactive Lattice-Confined Ru_2 Nitride by Photocrystallography. *J. Am. Chem. Soc.* **2017**, *139*, 2912–2915.
57. Timmer, G. H.; Berry, J. F. Electrophilic Aryl C–H Amination by Dimetal Nitrides: Correlating Electronic Structure with Reactivity. *Chem. Sci.* **2012**, *3*, 3038–3052.
58. Chakravarty, A. R.; Cotton, F. A.; Tocher, D. A. New Isomeric Form of the "$M_2(OC_5H_3NCl)_4$" Core: A Polar Arrangement of the Four 6-Chloro-2-hydroxypyridinato (chp) Ligands in a Chlorodiruthenium(II,III) Complex, $Ru_2Cl(chp)_4$. *Inorg. Chem.* **1985**, *24*, 1263–1267.
59. Bartocci, C.; Scandola, F. The Photoredox Decomposition of a Platinum(II) Complex Ion. *J. Chem. Soc. D* **1970**, 531a–531a.
60. Reed, J. L.; Gafney, H. D.; Basolo, F. Photochemical Reactions of the Azidopentaamminerhodium(III) ion. Nitrene and Redox Reaction Paths. *J. Am. Chem. Soc.* **1974**, *96*, 1363–1369.
61. Brown, G. M.; Callahan, R. W.; Meyer, T. J. Thermal and Light-Induced Decomposition of Azido(bis-2,2'-bipyridine) Complexes of Ruthenium(III). *Inorg. Chem.* **1975**, *14*, 1915–1921.
62. Ho, C. M.; Leung, H. C.; Wu, S.; Low, K. H.; Lin, Z.; Che, C. M. Thermal and Photochemical Reactions of Azidoruthenium(III) Complexes of Macrocyclic Tertiary Amines and the Structure of the (Phosphoraniminato)ruthenium(III) Complex *trans*-$[Ru(14\text{-}TMC)(N_3)(NPPh_3)]^+$. *Eur. J. Inorg. Chem.* **2012**, 151–159.
63. Lutterman, D. A.; Degtyareva, N. N.; Johnston, D. H.; Gallucci, J. C.; Eglin, J. L.; Turro, C. Photoinduced One-Electron Reduction of Alkyl Halides by Dirhodium(II,II) Tetraformamidinates and a Related Complex with Visible Light. *Inorg. Chem.* **2005**, *44*, 5388–5396.
64. Reiher, M.; Kirchner, B.; Hutter, J.; Sellmann, D.; Hess, B. A. A Photochemical Activation Scheme of Inert Dinitrogen by Dinuclear Ru^{II} and Fe^{II} Complexes. *Chem. – Eur. J.* **2004**, *10*, 4443–4453.
65. Neyman, K. M.; Nasluzov, V. A.; Hahn, J.; Landis, C. R.; Rösch, N. Density Functional Study of N_2 Activation by Molybdenum (III) Complexes. Unusually Strong Relativistic Effects in 4d Metal Compounds. *Organometallics* **1997**, *16*, 995–1000.
66. Graham, D. C.; Beran, G. J.; Head-Gordon, M.; Christian, G.; Stranger, R.; Yates, B. F. Nitrogen Activation via Three-Coordinate Molybdenum Complexes: Comparison of Density Functional Theory Performance with Wave Function Based Methods. *J. Phys. Chem. A* **2005**, *109*, 6762–6772.
67. Klopsch, I.; Finger, M.; Würtele, C.; Milde, B.; Werz, D. B.; Schneider, S. Dinitrogen Splitting and Functionalization in the Coordination Sphere of Rhenium. *J. Am. Chem. Soc.* **2014**, *136*, 6881–6883.
68. Silantyev, G. A.; Förster, M.; Schluschaß, B.; Abbenseth, J.; Würtele, C.; Volkmann, C.; Holthausen, M. C.; Schneider, S. Dinitrogen Splitting Coupled to Protonation. *Angew. Chem., Int. Ed.* **2017**, *56*, 5872–5876.
69. Christian, G.; Driver, J.; Stranger, R. Dinitrogen Activation in Sterically-Hindered Three-Coordinate Transition Metal Complexes. *Faraday Discuss.* **2003**, *124*, 331–341.
70. Tran, B. L.; Pinter, B.; Nichols, A. J.; Konopka, F. T.; Thompson, R.; Chen, C. H.; Krzystek, J.; Ozarowski, A.; Telser, J.; Baik, M.-H.; Meyer, K.; Mindiola, D. J. A Planar Three-Coordinate Vanadium(II) Complex and the Study of Terminal Vanadium Nitrides from N_2: a Kinetic or Thermodynamic Impediment to N–N Bond Cleavage? *J. Am. Chem. Soc.* **2012**, *134*, 13035–13045.
71. Brookes, N. J.; Graham, D. C.; Christian, G.; Stranger, R.; Yates, B. F. The Influence of Peripheral Ligand Bulk on Nitrogen Activation by Three-Coordinate Molybdenum complexes—A Theoretical Study Using the ONIOM Method. *J. Comput. Chem.* **2009**, *30*, 2146–2156.
72. Arashiba, K.; Eizawa, A.; Tanaka, H.; Nakajima, K.; Yoshizawa, K.; Nishibayashi, Y. Catalytic Nitrogen Fixation via Direct Cleavage of Nitrogen–Nitrogen Triple Bond of Molecular Dinitrogen Under Ambient Reaction Conditions. *Bull. Chem. Soc. Jpn.* **2017**, *90*, 1111–1118.
73. Caselli, A.; Solari, E.; Scopelliti, R.; Floriani, C.; Re, N.; Rizzoli, C.; Chiesi-Villa, A. Dinitrogen Rearranging over a Metal–Oxo Surface and Cleaving to Nitride: From the End-On to the Side-On Bonding Mode, to the Stepwise Cleavage of the N≡N Bonds Assisted by Nb^{III}-calix[4]arene. *J. Am. Chem. Soc.* **2000**, *122*, 3652–3670.
74. Liu, C. G.; Liu, S.; Zheng, T. Computational Study of Metal–Dinitrogen Keggin-Type Polyoxometalate Complexes $[PW_{11}O_{39}M^{II}N_2)]^{5-}$ (M = Ru, Os, Re, Ir): Bonding Nature and Dinitrogen Splitting. *Inorg. Chem.* **2015**, *54*, 7929–7935.
75. Curley, J. J.; Cook, T. R.; Reece, S. Y.; Müller, P.; Cummins, C. C. Shining Light on Dinitrogen Cleavage: Structural Features, Redox Chemistry, and Photochemistry of the Key Intermediate Bridging Dinitrogen Complex. *J. Am. Chem. Soc.* **2008**, *130*, 9394–9405.
76. Katayama, A.; Ohta, T.; Wasada-Tsutsui, Y.; Inomata, T.; Ozawa, T.; Ogura, T.; Masuda, H. Dinitrogen-Molybdenum Complex Induces Dinitrogen Cleavage by One-Electron Oxidation. *Angew. Chem., Int. Ed.* **2019**, *58*, 11279–11284.
77. Bruch, Q. J.; Connor, G. P.; Chen, C. H.; Holland, P. L.; Mayer, J. M.; Hasanayn, F.; Miller, A. J. M. Dinitrogen Reduction to Ammonium at Rhenium Utilizing Light and Proton-Coupled Electron Transfer. *J. Am. Chem. Soc.* **2019**, *141*, 20198–20208.
78. Pucino, M.; Allouche, F.; Gordon, C. P.; Wörle, M.; Mougel, V.; Copéret, C. A Reactive Coordinatively Saturated Mo(III) Complex: Exploiting the Hemi-Lability of Tris(*tert*-butoxy) Silanolate Ligands. *Chem. Sci.* **2019**, *10*, 6362–6367.
79. Bendix, J.; Anthon, C.; Schau-Magnussen, M.; Brock-Nannestad, T.; Vibenholt, J.; Rehman, M.; Sauer, S. P. A. Heterobimetallic Nitride Complexes from Terminal Chromium(V) Nitride Complexes: Hyperfine Coupling Increases with Distance. *Angew. Chem., Int. Ed.* **2011**, *50*, 4480–4483.
80. Cotton, F. A.; Kim, Y.; Yokochi, A. Regioisomerism Displayed by the 6-Chloro-2-oxopyridinate Complexes of Ru_2^{4+} and Ru_2^{5+}. *Inorg. Chim. Acta* **1995**, *236*, 55–61.
81. Brown, T. R.; Dolinar, B. S.; Hillard, E. A.; Clerac, R.; Berry, J. F. Electronic Structure of Ru_2(II,II) Oxypyridinates: Synthetic, Structural, and Theoretical Insights into Axial Ligand Binding. *Inorg. Chem.* **2015**, *54*, 8571–8589.
82. Ring, S.; Meijer, A. J.; Patmore, N. J. Structural, Spectroscopic and Theoretical Studies of a Diruthenium(II,II) Tetraformamidinate that Reversibly Binds Dioxygen. *Polyhedron* **2016**, *103*, 87–93.

Authors are required to submit a graphic entry for the Table of Contents (TOC) that, in conjunction with the manuscript title, should give the reader a representative idea of one of the following: A key structure, reaction, equation, concept, or theorem, etc., that is discussed in the manuscript. Consult the journal's Instructions for Authors for TOC graphic specifications.

Insert Table of Contents artwork here

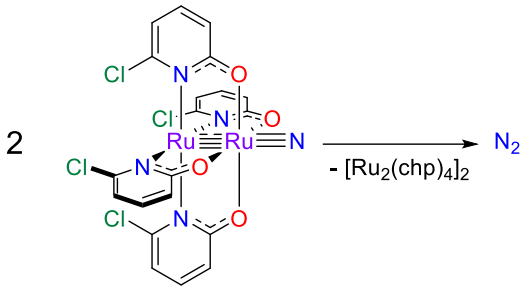

$Ru_2(chp)_4N$